Improved Vehicle Handling through Wheel-Individual Vertical Actuation in Low-Friction Conditions

Citation for the original published paper (version of record):

Ashok, N., Gelso, E., Sadeghi Kati, M. et al (2026). Improved Vehicle Handling through Wheel-Individual Vertical Actuation in Low-Friction Conditions. Proceedings of the 17th International Symposium on Advanced Vehicle Control (AVEC ’26)

(article starts on next page)

Improved Vehicle Handling through Wheel-Individual Vertical Actuation in Low-Friction Conditions

Nrupathunga Ashok[1,2], Esteban R. Gelso[1], Leo Laine[1,3], Maliheh Sadeghi Kati[1], Mats Jonasson[3], Jonas Fredrkisson[2]

1) Volvo Trucks Technology & Industrial Division, Gothenburg, 40508, Sweden
2) Department of Electrical Engineering, Chalmers University of Technology, Gothenburg, 41296 Sweden
3) Department of Mechanical Engineering, Chalmers University of Technology, Gothenburg, 41296 Sweden
(Corresponding author: nrupathunga.ashok@volvo.com)

Abstract: This paper presents the development and validation of a dynamic motion model of an electric bus equipped with a hydro-pneumatic suspension system. The model is validated against experimental data from a real electric bus and is used to evaluate the effects of individual-wheel vertical actuation on vehicle behavior under low-friction road conditions. Simulations and experimental results demonstrate that the proposed model can represent key vehicle dynamics with sufficient accuracy to assess vehicle performance and support the development of safer, more robust suspension systems for electric buses. The study also examines how individual wheel-suspension actuation improves handling and acceleration performance of electric buses.

Keywords: Vehicle Dynamics, Vehicle Control, Chassis, Wheel vertical actuation, Hydro-pneumatic Suspension, Low-friction conditions

1. Introduction

Heavy-duty vehicles operate under demanding conditions where stability, traction, ride quality, and handling are strongly influenced by load transfer and tire-road interaction. Suspension systems play a critical role in managing these factors by controlling vehicle body motion, regulating dynamic wheel loads, and maintaining favorable tire-road contact. Consequently, suspension design and control have been the subject of extensive research, particularly with the emergence of advanced active suspension technologies aimed at improving ride comfort, handling performance, and vehicle safety, as comprehensively reviewed in [(1)].

For electric and heavy-duty vehicles, maintaining optimal tire utilization is particularly important because vehicle efficiency and dynamic performance are closely coupled. Research on wheel slip control has demonstrated that effective management of tire forces can improve both traction capability and energy efficiency by operating the tire near its optimal slip region [(2)]. However, the achievable traction force is fundamentally limited by the vertical load acting on the tire, highlighting the importance of suspension systems in influencing vehicle performance beyond traditional ride comfort objectives.

These challenges become even more significant under winter driving conditions, where the available tire-road friction is substantially reduced. The review by Lu et al. [(3)] showed that vehicle traction performance on snowy and icy surfaces is highly sensitive to tire characteristics, vehicle loading, and the distribution of normal forces between the wheels. For heavy-duty vehicles, variations in dynamic wheel loads caused by suspension motion and load transfer can therefore have a significant impact on the available longitudinal force and overall vehicle mobility.

To address variations in vehicle loading, heavy-duty vehicles have employed hydro-pneumatic and air suspension systems for decades. These systems offer load-leveling functionality and the ability to adjust chassis height by redistributing loads between axles on multi-axle vehicles. However, due to slow actuation and limited capability to control vertical force at the individual wheels, their potential to improve handling, particularly on two-axle heavy-duty vehicles, has received limited attention. The relationship between suspension dynamics, tire loading, and vehicle control is particularly relevant in low-μ conditions, where even small changes in vertical load can influence the generation of longitudinal tire forces. This motivates the investigation of wheel-individual vertical force actuation as a potential means of improving vehicle performance on low-friction surfaces.

Therefore, this paper investigates whether wheel-individual vertical actuation can improve the longitudinal performance of a heavy-duty vehicle operating under low-μ conditions. To answer this question, open-loop simulation studies are conducted using a high-fidelity vehicle model equipped with a hydro-pneumatic suspension system developed in IPG TruckMaker [(4)]. The suspension model is validated against experimental measurements obtained from an electric city bus, providing a realistic platform for evaluating the influence of active wheel-load manipulation on vehicle traction performance.

Fig. 1: Test Vehicle used for modeling, simulation and real tests: 4×2 battery-electric city bus

2. Test Vehicle Specification

The test vehicle is a 4×2 battery-electric city bus, shown in Figure 1, with rear-wheel drive and an open differential. It is equipped with a hydro-pneumatic suspension system capable of individually actuated wheels. Hydro-pneumatic suspension is considered due to its improved force and position control at individual wheels, high load-carrying capacity, and compact form-factor. The suspension employs double-acting cylinders at each wheel, cross-coupled so that the piston side of one cylinder is connected to the rod side of the cylinder on the other side of the axle; this stabilizes roll motion, which is otherwise provided by the anti-roll bar in conventional suspension systems. Each corner has a solenoid-controlled orifice that provides damping and diaphragm accumulators containing pressurized Nitrogen gas that provide spring force. The volume and pre-charge pressure of the accumulators are tuned to provide the desired ride characteristics. Each axle has a leveling manifold that is connected to a pump and reservoir. The system is equipped with stroke sensors for relative wheel displacement and pressure sensors to estimate the vertical load at each wheel. In addition, the vehicle is instrumented with a steering-wheel angle sensor, a wheel-based vehicle speed sensor, and an inertial measurement unit (IMU) mounted on the floor at the vehicle's geometric center in the XY plane.

3. Vehicle Modeling

The MB Citaro O345 2003 model in IPG TruckMaker is used as the base vehicle. The hydro-pneumatic suspension system is added in Simulink, and the driveline is converted to electric and parametrized to match the test vehicle. The vehicle model parameters used are shown in Table 1.

Table 1: Vehicle and driveline parameters

Parameter	Value	Unit
Vehicle total mass	11587	kg
Center of gravity, x-position	5.58	m
Center of gravity, y-position	0.07	m
Center of gravity, z-position	0.69	m
Axle load front	4364	kg
Axle load rear	7223	kg
Un-sprung mass front	500	kg
Un-sprung mass rear	700	kg
Wheel base	5.82	m
Track Width	2	m
Mechanical power	180	kW
Maximum torque	450	Nm
Maximum rotational speed	12000	rpm
Gear ratio 1	7.99	-
Gear ratio 2	5.87	-
Differential ratio	4.72	-

3.1. Suspension Modeling

The suspension modeled in Simulink follows the same physical principles as [5], and the hydraulic layout is shown in Figure 2. The Simulink model receives suspension cylinder stroke information from IPG TruckMaker and provides actuator force as a function of system pressure:

$$F_l = P_{pl} \cdot A_{ps} - P_{rl} \cdot A_{rs}, \tag{1}$$

$$F_r = P_{pr} \cdot A_{ps} - P_{rr} \cdot A_{rs}, \tag{2}$$

where F_l and F_r are the left and right-side cylinder forces, respectively, A_{ps} is the piston effective area, A_{rs} is the rod-side or annular effective area, P_{pl} and P_{pr} are the left and right-side piston-end fluid pressures, respectively, P_{rl} and P_{rr} are the left and right-side rod-end fluid pressures, respectively. The process is assumed isothermal due to the low-frequency excitation, and the suspension system pressures can be computed as:

$$P_{pl} = \frac{P_0 \cdot V_0}{V_0 + A_{ps} \cdot z_l - A_{rs} \cdot z_r - V_l}, \tag{3}$$

$$P_{pr} = \frac{P_0 \cdot V_0}{V_0 + A_{ps} \cdot z_r - A_{rs} \cdot z_l - V_r}, \tag{4}$$

$$P_{rl} = P_{pr} + dP_{ol} + dP_p, \tag{5}$$

$$P_{rr} = P_{pl} + dP_{or} + dP_p, \tag{6}$$

where P_0 and V_0 are the accumulator pre-charge pressure and volume, respectively, and V_l and V_r are the amount of oil added or removed from the left and right suspension circuits through the leveling manifold, respectively. The volumes are obtained by integrating the volumetric flow rates across the leveling manifolds. z_l and z_r are the left and right-side cylinder levels, respectively; dP_{ol} and dP_{or} are the pressure drops across the left and right-side damping manifolds, respectively, and dP_p is the pressure drop in the hydraulic pipes. The pressure drop across the orifice is calculated using the standard incompressible orifice flow equation, given by:

$$dP_{ol} = sign(\dot{V}_l) \cdot \frac{8 \cdot \rho \cdot \dot{V}_l^2}{\pi^2 \cdot C_d^2 \cdot D_{ol}^4}, \tag{7}$$

$$dP_{or} = sign(\dot{V}_r) \cdot \frac{8 \cdot \rho \cdot \dot{V}_r^2}{\pi^2 \cdot C_d^2 \cdot D_{or}^4}, \tag{8}$$

$$\dot{V}_l = \dot{z}_l \cdot A_{rs}, \tag{9}$$

$$\dot{V}_r = \dot{z}_r \cdot A_{rs}. \tag{10}$$

where $\dot{V}_l$ and $\dot{V}_r$ are the volumetric flow rates through the left and right-side damping orifices, respectively, and D_{ol} and D_{or} are the left and right-side orifice diameters, respectively. The pressure drop in the pipe, dP_p, is calculated using the Hagen–Poiseuille equation written in terms of volumetric flow rate as follows:

$$dP_p = \frac{128 \cdot \mu \cdot \dot{V} \cdot L_p}{\pi \cdot D_p^4}, \tag{11}$$

where μ is the fluid viscosity, $\dot{V}$ is the volumetric flow rate through the pipe, which is the same as the flow through the damping orifice of the respective side, L_p is the pipe length, and D_p is the pipe inner diameter. It should be noted that the pipe length is chosen to account for pressure drops in the real system caused by couplings, bends, and other resistances. The sign convention for the level is negative in cylinder compression.

4. Suspension Control Strategy

The suspension controller used in this paper focuses on axle-motion actuation, and the normal forces generated at the wheels are partly attributable to this actuation. Axle roll and axle heave are the possible motion requests, which are then decomposed into individual wheel-level targets. The combination of these controls results in vehicle heave, pitch, and roll motions. Since the vehicle has two axles, no significant normal load distribution can be actuated along the longitudinal axis. However, by applying opposite roll angles at the two axles, chassis torsion can be used to actuate load

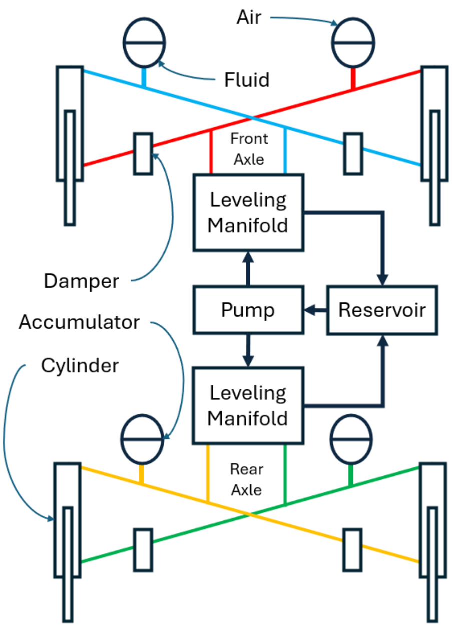

Fig. 2: Schematic of the hydro-pneumatic suspension system

distribution along the diagonals. Provided the axle heave and/or roll requests, the equations for the individual wheel-level references are as follows:

$$z_l^* = z_{axle}^* + \frac{cc \cdot tan(\phi_{axle}^*)}{2}, \tag{12}$$

$$z_r^* = z_{axle}^* - \frac{cc \cdot tan(\phi_{axle}^*)}{2}, \tag{13}$$

where z_{axle}^* and ϕ_{axle}^* are the heave and roll requests, respectively, for a given axle, and z_l^* and z_r^* are the left and right-side cylinder stroke reference values, respectively, for that axle. Once the references are calculated, the oil volumes that need to be added or removed from the left and right sides are calculated as follows:

$$V_l^* = (z_l^* - z_l) \cdot A_{ps} - (z_r^* - z_r) \cdot A_{rs}, \tag{14}$$

$$V_r^* = (z_r^* - z_r) \cdot A_{ps} - (z_l^* - z_r) \cdot A_{rs}, \tag{15}$$

where z_l and z_r are the current cylinder stroke values for the left and right sides, respectively. The left and right valve actuation times are calculated as:

$$t_l = \frac{V_l^*}{\dot{V}_v}, \tag{16}$$

$$t_r = \frac{V_r^*}{\dot{V}_v}, \tag{17}$$

where $\dot{V}_v$ is the volumetric flow rate of the constant-flow leveling valve.

The controller uses a dead-band around the reference value to improve stability and reduce chattering. The static normal loads at the wheels are calculated using the cylinder forces as:

$$Fz_l = F_l \cdot \frac{R_1}{2} + F_r \cdot \frac{R_2}{2} + g \cdot \frac{m_u}{2}, \tag{18}$$

$$Fz_r = F_r \cdot \frac{R_1}{2} + F_l \cdot \frac{R_2}{2} + g \cdot \frac{m_u}{2}, \tag{19}$$

$$R_1 = 1 + \frac{cc}{tw}, \tag{20}$$

$$R_2 = 1 - \frac{cc}{tw}, \tag{21}$$

where Fz_l and Fz_r are the left and right-side static wheel normal loads, respectively, R_1 and R_2 are force ratios, respectively, cc is the cylinder-cylinder distance, tw is the track width, m_u is the unsprung mass, F_l and F_r are the left and right-side cylinder forces, respectively and are calculated using the system pressures as:

$$F_l = P_l \cdot A_{ps} - P_r \cdot A_{rs}, \tag{22}$$

$$F_r = P_r \cdot A_{ps} - P_l \cdot A_{rs}, \tag{23}$$

where P_l and P_r are the left and right-side system pressures, respectively.

5. Test Scenarios

The experimental vehicle is tested in northern Sweden at the Colmis test facility in winter. The suspension settings, which are the different axle roll values requested and the resulting wheel normal loads tested in simulation and experiment, are shown in Table 2, and the findings of these tests are presented in this section. In the baseline setting (S_0), the wheel normal loads on the left side are higher due to the presence of the driver's seat, hydraulic pump, oil tank, and other components present on that side of the vehicle. Trim loads are used in IPG to match the wheel normal loads of the simulation model to that of the real vehicle.

Fig. 3: Circular test track at Colmis proving ground [6]

Table 2: Suspension settings and the resulting wheel normal loads

Suspension setting	S_0	S_1	S_2	S_3	Unit
Front left, $F_{z_{fl}}$	24.9	17.6	24.5	26.1	kN
Front right, $F_{z_{fr}}$	17.9	25.3	18.3	16.8	kN
Rear left, $F_{z_{rl}}$	36.1	44.9	36.6	34.9	kN
Rear right, $F_{z_{rr}}$	34.6	25.9	34.1	35.9	kN
Front axle roll angle	0	-1.5	-2	2	deg
Rear axle roll angle	0	1.5	-2	2	deg

5.1. Steady-State Cornering Test

Rolling into a corner (S_2) improves perceived stability and comfort [7], while rolling out (S_3) is included to better understand how the direction of body roll influences cornering behavior. The test vehicle is driven counterclockwise on the inner circle of the dynamic circle lake track at the Colmis facility, as shown in Figure 3. The track surface is made of packed snow (μ = 0.2 to 0.4) with a diameter of 200 m. Suspension settings S_0, S_2, and S_3 are tested, and the findings are discussed below.

Figure 4 and Figure 5 compare the longitudinal speed and steering wheel angle, respectively, between simulation and experiment, which shows that the same maneuvers were conducted in both environments. The deviation in steering wheel angle in the experimental data is due to the vehicle being driven onto the circular path from inside the circle.

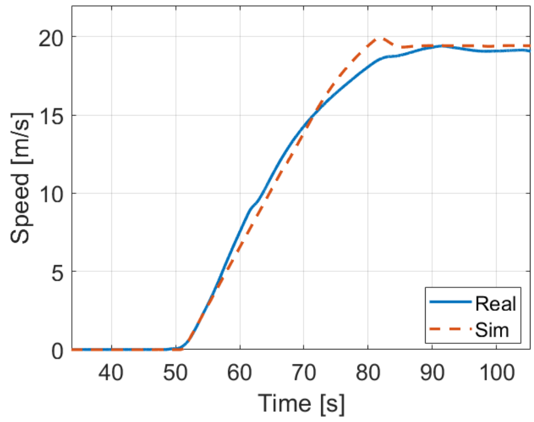

Fig. 4: Vehicle speed in test vehicle and simulation

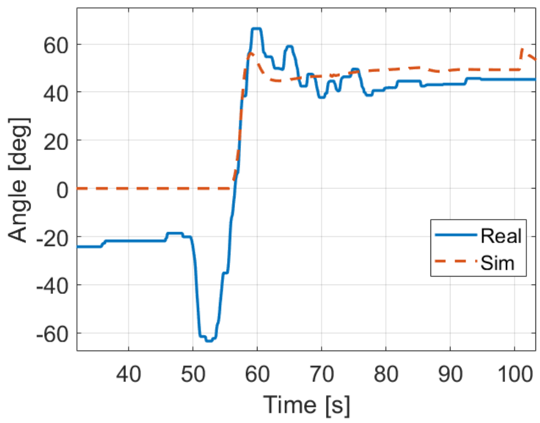

Fig. 5: Steering wheel angle for test vehicle and simulation

Figure 7 shows the comparison of front and rear-axle cylinder strokes, respectively, and also the comparison of front and rear-axle cylinder pressures, respectively, between simulation and experiment. The test begins with the vehicle accelerating up to 70 km/h from stand-still, this is observed in the plots where the cylinder stroke values, z_{fl} and z_{fr}, increase and system pressures, P_{fl} and P_{fr}, drop on the front axle, while the cylinder stroke values decrease and system pressures increase on the rear axle due to load transfer from the front to rear caused by longitudinal acceleration at around 50 s. As the vehicle gains speed while driving around the circle counterclockwise, lateral load transfer due to centripetal force causes the left-side system pressures to drop while the right-side system pressures increase. The body roll due to lateral acceleration is also reflected in the cylinder stroke plots, where the left-side cylinder stroke values increase, and the right-side values decrease, corresponding to a positive body roll angle. The stroke and pressure reach steady state when the vehicle reaches 70 km/h. The plots show a good correlation between the model and the real vehicle during

Fig. 6: Split-friction test track at Colmis proving ground[6]

the steady-state cornering maneuver.

In both the simulation results and the experiment, it is noted that the mean steering wheel angle required to maintain the course is lower in the suspension setting where the vehicle rolls toward the center of the circle, and higher in the setting where the suspension rolls outward, compared with the baseline. The mean steering wheel angles for the maneuvers are shown in Table 3. This is attributed to the suspension kinematics, where the axles rotate about the Z axis as a function of axle roll about the X axis, creating a 'skateboard' effect when the vehicle rolls toward the center of the circle and thereby requiring a lower steering wheel angle than the baseline effect. Whereas rolling outward has the opposite effect.

Table 3: Mean steering wheel angle in circle driving

Set-up	S0	S2	S3	Unit
Simulation	49.2	44.3	54.4	deg
Experiment	43.8	36.7	62.1	deg

The subjective feeling of a passenger during the experiments is that S_2 was more comfortable and S_3 was less comfortable than S_0, this is in line with studies conducted in [7]. This is because gravity counteracts the centrifugal force and the passenger is pushed into the seat rather than sliding out when cornering, similar to driving on a banked curve. The deviation in mean steering wheel angle between simulation and experiment for the different tests may be attributed to differences in kinematics and compliance parameters.

5.2. Split-μ Startability Test

Startability tests are performed on the split-μ track at Colmis proving ground shown in Figure 6, with the front-left and rear-left wheels on polished ice (μ = 0.1 to 0.2) and the remaining wheels on dry asphalt (μ = 0.8 to 0.9). Increasing the normal load on the driven wheel located on the low-μ side of a split friction surface should improve traction and longitudinal acceleration of a vehicle with an open differential. The hypothesis is tested using settings S_0 and S_1. The vehicle starts from standstill with the steering wheel held in the straight-ahead position. A step input of 100 % throttle is applied, and the longitudinal speed of the vehicle is recorded. The speed achieved after 10 s is used as the key performance metric. The friction coefficient used in the simulation is 0.05, and the results from real-world tests and simulation are shown in Table 4.

For the friction conditions considered in this test, increasing the normal load of the wheel on the low μ surface by 9 kN improves startability by 17% and 31% in simulation and experiment, respectively. The difference in performance between simulation and

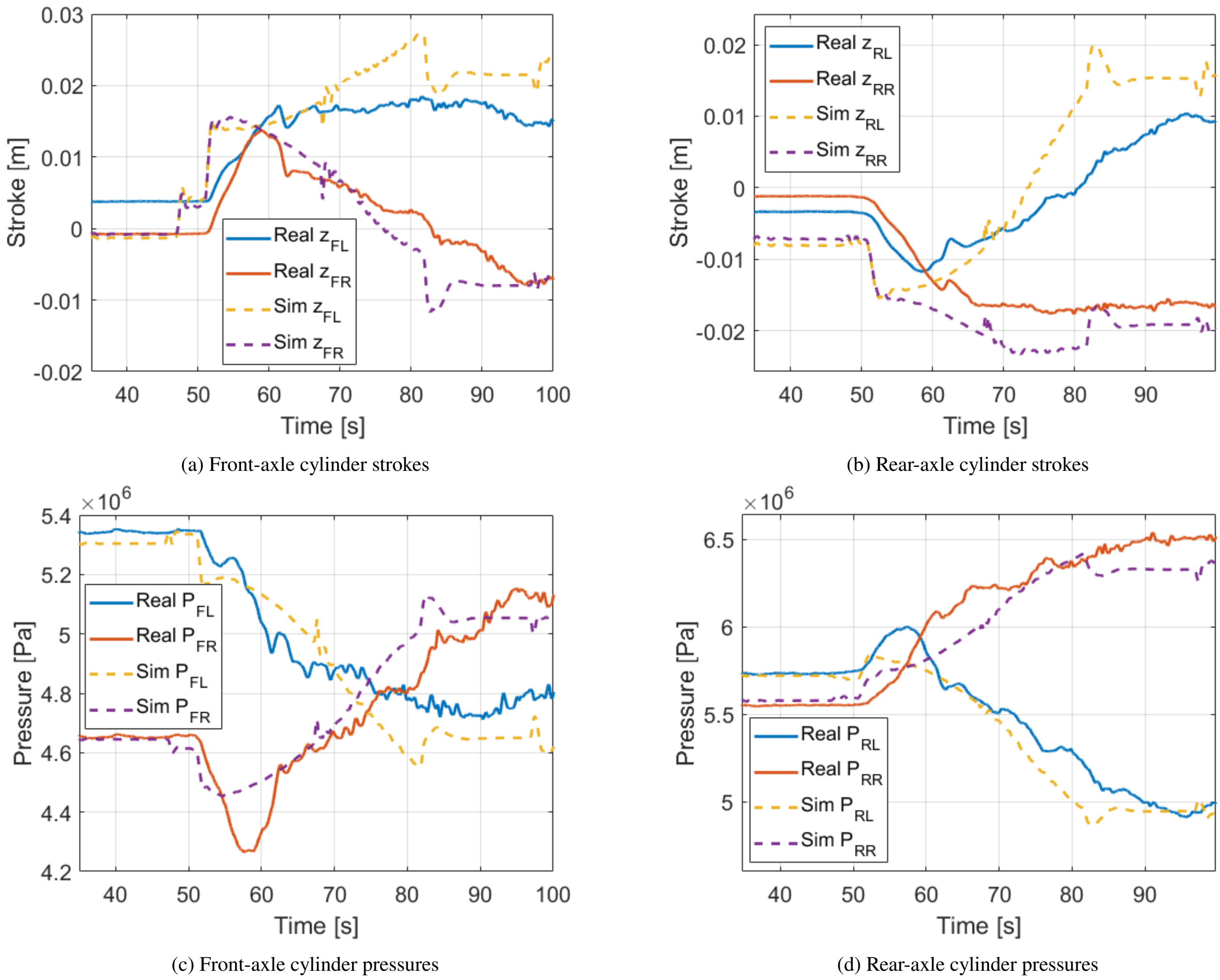

(a) Front-axle cylinder strokes

(b) Rear-axle cylinder strokes

(c) Front-axle cylinder pressures

(d) Rear-axle cylinder pressures

Fig. 7: Steady-state cornering test results for baseline setting, S_0, simulations vs real test

Table 4: Vehicle speed measured after 10 s during split-friction startability tests

Set-up	S_0	S_1	Unit
Simulation	3.5	4.1	m/s
Experiment	3.5	4.6	m/s

experiment is likely due to variations in the friction coefficient along the real vehicle's driven path.

6. Conclusion

The vehicle model with hydro-pneumatic suspension is validated against experimental data from a real electric city bus using suspension cylinder stroke and system pressures for steady-state circular driving on packed snow. In addition, both simulation and real tests show that control of body roll angle affects driver steering effort. The open-loop tests indicate that individual wheel-suspension control can improve acceleration performance in vehicles with an open differential under split-friction conditions. Future work will focus on validating the model for dynamic maneuvers and on exploring normal-force control at the wheels rather than motion control at the axles. The validated model will then be used to investigate closed-loop control of individual wheel suspensions to balance multiple objectives during transient and steady-state maneuvers.

7. Acknowledgments

The authors would like to acknowledge financial support from the FFI – Strategic Vehicle Research and Innovation programme, in the project *Electrified heavy-duty wheel corner design for optimized motion and force control*, P2025-01051, funded by the Swedish Energy Agency.

References

(1) M. Yu, S. A. Evangelou, and D. Dini, "Advances in active suspension systems for road vehicles," 2024.
(2) K. Nam, Y. Hori, and C. Lee, "Wheel slip control for improving traction-ability and energy efficiency of a personal electric vehicle," *Energies*, vol. 8, 2015.
(3) J. J. Lu, "Vehicle traction performance on snowy and icy surfaces," *Transportation Research Record*, 1996.
(4) I. A. GmbH. (2025) Truckmaker simulation software. [Online]. Available: https://www.ipg-automotive.com
(5) J. Zou, X. Guo, M. A. Abdelkareem, L. Xu, and J. Zhang, "Modelling and ride analysis of a hydraulic interconnected suspension based on the hydraulic energy regenerative shock ab-

sorbers," *Mechanical Systems and Signal Processing*, vol. 127, 2019.

(6) Colmis. (2023) Colmis proving ground, arjeplog. [Online]. Available: https://colmis.com/test-tracks/

(7) Y. Zheng, B. Shyrokau, T. Keviczky, M. A. Sakka, and M. Dhaens, "Curve tilting with nonlinear model predictive control for enhancing motion comfort," *IEEE Transactions on Control Systems Technology*, vol. 30, 2022.